TECHNISCHE MECHANIK
an open access journal

journal homepage: www.ovgu.de/techmech

Tech. Mech., Vol. 39, Is. 3, (2019), 282–297

Received: 26.08.2019
Accepted: 26.09.2019
Available online: 01.10.2019

Simulating and Evaluating Synchronized Vibrations in Macroscopic Tribological Contacts

J. H. Merlis[1] and G.-P. Ostermeyer[1]*

[1] TU Braunschweig, Institute of Dynamics and Vibrations, Schleinitzstraße 20, 38106 Braunschweig, Germany

Abstract: High-frequency synchronized vibrations in the friction contact constitute one known triggering mechanism of certain types of NVH phenomena in automotive brakes. Towards an improved understanding of the associated physical processes, vibrations of contact patches in the tribological boundary layer are computed using the Abstract Cellular Automaton simulation program. Various studies are presented, each illustrating unique types of local phenomena and observable global behaviors. For example, simulations are carried out on multiple timescales, enabling investigations into the emergence of global patch coverage states and the resulting vibrational behavior in the tribological contact. Relevant means for analyzing and interpreting these results are introduced, including a qualitative visual representation scheme, frequency analyses of the global coefficient of friction, and a new method for quantifying the synchronization of multiple oscillating bodies.

Keywords: cellular automaton, simulation, boundary layer dynamics, patch dynamics, synchronized vibrations, brake squeal

1 Introduction

Friction-induced vibrations are prevalent in many fields, and are often linked to unwanted noise, vibration and harshness (NVH) events Leine et al. (1998). One widely researched example is the NVH behavior of automotive braking systems, e.g. high-frequency squeal Hamabe et al. (1999); Van de Vrande et al. (1999); Hoffmann et al. (2002); Popp (2005); Ostermeyer (2008, 2010); Wernitz and Hoffmann (2012). Of the many phenomena related to brake squeal, synchronized vibrations in the friction contact have been identified as one potential triggering mechanism Ostermeyer (2010).

Measurement-based investigations can offer insights into such synchronized vibrations. They reveal isolated information regarding the behavior of a particular complete test system under specific conditions, sometimes leading to new insights into trends within limited parameter ranges. In order to better understand the fundamental tribological phenomena within the contact area, approaches combining theory and simulations are often employed.

The *Abstract Cellular Automaton* (ACA) simulation program is used to simulate the entire tribological contact between a brake pad and disc Ostermeyer and Merlis (2018). Based on patch theory Ostermeyer (2001), the ACA simulates the development, destruction, and further dynamics of contact structures in the boundary layer. This enables an efficient, targeted analysis of the elements of the brake system that predominantly influence the global tribological behavior, while also allocating appropriate computational resources to further system components Ostermeyer and Merlis (2018).

The current work presents studies performed using the ACA towards analyzing the high-frequency (HF, on the order of 1 kHz and above) vibration states that occur in the friction contact of automotive brakes, as discussed for example in Wernitz and Hoffmann (2012); Ostermeyer (2010); Otto and Ostermeyer (2018). To this end, the vibrations of the contact patches are modeled and simulated using this tool.

A particular focus is set on the synchronized stick-slip-like motion of these contact areas along the direction of friction. While synchronization has already been the subject of research in various contexts Lachaux et al. (1999); Sinkkonen et al. (1995); Palva et al. (2005); Slagter et al. (2009); Stefański et al. (2007); Perlikowski et al. (2008), this work aims to analyze synchronized friction-induced vibrations with the complexity of an entire pad-disc contact. The authors presuppose that appreciable synchronized vibrations of the patches can occur in the tribological boundary layer, and that the resulting HF oscillatory character of the global coefficient of friction can trigger undesired NVH events in automotive brake systems, as supported by Ostermeyer (2008); Lee and Gesch (2009). For example, synchronously oscillating patches may excite vibrations in the brake disc, which can then generate audible pressure fluctuations. Under these assumptions, such synchronization states are detected and characterized in this work. The stability of these phenomena is not considered within the scope of this work.

First, the simulation program and the associated models used in these investigations are presented and explained. A full pad-disc contact is simulated on multiple time scales, modeling both the development and HF vibrations of contact structures. A friction model is chosen which induces relevant vibrations, enabling a simple numerical investigation of emergent synchronization states. A new means of quantifying the synchronization of many oscillating bodies is then introduced. Results of the simulative studies and analyses are then presented. Finally, the work is summarized and potential steps for further advancements are suggested.

* E-mail address: gp.ostermeyer@tu-braunschweig.de
doi: 10.24352/UB.OVGU-2019-025

2 Materials and Methods

2.1 Simulating Vibrations in Tribological Contacts

2.1.1 Simulation Program

The ACA efficiently simulates the tribological processes in brake contacts by concentrating the computational effort on the patches, and minimizing calculations of the surrounding surfaces Ostermeyer and Merlis (2015, 2018). By assigning each patch to an entry on a linked list, the ACA is capable of rapidly simulating the tribological behavior of the contact between a brake disc and an entire brake pad.
The fundamental functionality of the ACA on the long timescale (LF: $\Delta t = 0.01$ s) has been validated in previous works Ostermeyer and Merlis (2015, 2018). The ACA simulation program is capable of producing results comparable to those attained using classical, grid-based cellular automata Ostermeyer and Merlis (2015). It has also been shown that the ACA generates complex macroscopic friction behaviors with simple local friction assumptions. For example, thermoelastic instabilities have been successfully simulated with Coulomb friction implemented at all contact surfaces Ostermeyer and Merlis (2015, 2018), with good correspondence to documented measurement results Lee and Barber (1994); Severin and Dörsch (2001). The ACA enables explicit comparisons of the unique interactions between the dynamics of the effective friction radius, the coefficient of friction, the global braking torque, and the patches in the tribological interface Ostermeyer and Merlis (2018).
This work focuses on specialized investigations of patch vibration dynamics in the tribological contact. This is a known phenomenon, measured for example in Wernitz and Hoffmann (2012); Otto and Ostermeyer (2018). The ACA simulations will provide an aid towards investigating relevant synchronization states in detail. Within the scope of this work, this will be carried out on a strictly theoretical level for developing analysis methods. Physical measurements for motivating and verifying the specifics of the processes and phenomena will be the subject of future research.

2.1.2 Simulation Model

The simulations of friction-induced vibrations in the tribological boundary layer presented in this paper are based on the fundamental model of brake friction introduced in Ostermeyer (2001). The theory that contact plateaus, or "patches," are primarily responsible for the global friction behavior of brake systems has been the basis of several cellular automaton-based simulations of the associated boundary layer Ostermeyer and Müller (2008); Wahlström (2014). These programs focused on simulating the life cycles of several patches, and the resulting effects on the tribological system. Furthermore, in order to simulate friction-induced vibrations in brake systems, simplified lumped-mass models representing the contact plateaus (or micro contacts) and the associated elastic couplings have been implemented Ostermeyer (2008, 2010). These simulations typically assume a given patch coverage state in the boundary layer, and compute the vibrations within an area that is much smaller than that of a full-scale brake pad. The ACA is capable of combining these two approaches: the development of a patch coverage state is simulated for the entire contact between a brake pad and disc, and the resulting friction-induced vibrations are then computed.
As shown in Figure 1, a lumped element model based on the one presented in Ostermeyer (2010) is implemented, enabling analyses of the patches' vibrational behavior Ostermeyer and Merlis (2018).

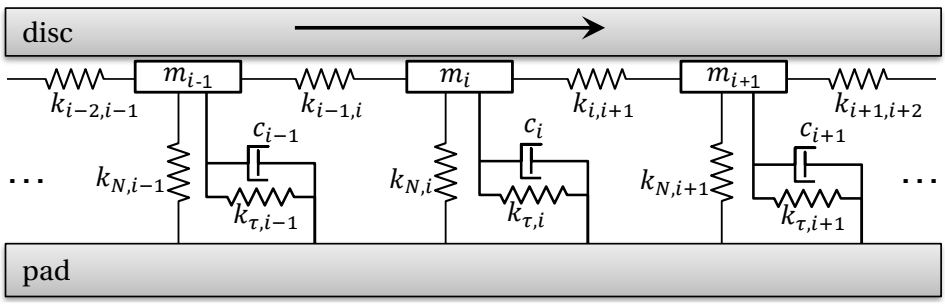

Fig. 1: Simplified Schematic Diagram of the Elastic Coupling Model for Patches P_{i-1}, P_i, and P_{i+1} (Potential Coupling between P_{i-1} and P_{i+1} not shown, reprinted from Ostermeyer and Merlis (2018))

The effective mass m_i of a given oscillating body encompasses the masses of the corresponding patch P_i and a small volume of the surrounding pad matrix material. This mass is approximated as proportional to the patch volume, typically within 0.75–3.0 mg. The effective spring stiffnesses in the normal (N) and tangential (T) directions are calculated as functions of the patch contact area A according to Eq. 1, Eq. 2, and Eq. 3

$$k_{i,N} = K_N \sqrt{A_i} \tag{1}$$

$$k_{i,T} = K_T \sqrt{A_i} \tag{2}$$

$$k_{i,j} = K_C \frac{\sqrt{A_i \cdot A_j}}{D_{0,ij}}, \tag{3}$$

with $K_N = 2.39 \cdot 10^9\,\mathrm{N\,m^{-2}}$, $K_T = 1.87 \cdot 10^9\,\mathrm{N\,m^{-2}}$, and $K_C = 7.96 \cdot 10^8\,\mathrm{N\,m^{-2}}$ based on the results of finite element method (FEM) parameter studies. The elastic coupling between two patches is neglected if the unloaded distance between them $D_{0,ij}$ exceeds 5 mm Ostermeyer and Merlis (2018).

This spring stiffness model reflects the assumption that the patches are cylindrical in form. This is consistent with the overarching modeling approach of the ACA, in which the shape of the patches is not taken into account. This approximation is considered adequate as a first approach. In the future, a more detailed spring stiffness model may be implemented, e.g. based on the Boussinesq-Cerruti solution Love (1892); Peng and Zhou (2012).

In the ACA, patches are elastically coupled to all neighboring patches within the aforementioned unloaded distance. Therefore, a spring $k_{i-1,i+1}$ could also be in effect, directly coupling patch P_{i-1} with P_{i+1} (not shown in Figure 1). This elastic coupling is implemented based on the proximity of neighboring patches along the two-dimensional boundary layer. The forces and displacements in the radial direction, perpendicular to the local relative motion of the disc, are neglected. Thus, the complete three-dimensional system is used towards establishing the conditions of the elastic coupling between patches, and the dynamic vibration analysis is implemented based on the two-dimensional system shown in Figure 1, neglecting vibrational effects and explicit couplings between patches in the normal direction Ostermeyer and Merlis (2018). For a simple consideration of a slightly damped system, the damping constants c are selected such that the damping ratio of each patch is equal to 10^{-6}. Patches are assumed to be small relative to the brake disc; the disc's rotation effectively results in a translational excitation on the patches' surfaces.

In physical systems, vibrations in the contact can be induced via various phenomena, for example mode coupling and stick-slip. It is supposed that patches exhibit micro stick-slip behavior as a result of a constant static friction coefficient which is greater than that of kinetic friction. This "true" stick-slip behavior is numerically challenging to implement on the scale of a full pad with hundreds or thousands of patches. To simulate this in a numerically sound and computationally achievable way, friction between the patches and disc is approximated with a falling friction curve over sliding speed, as shown in Eq. 4 and Figure 2. The macroscopic friction behavior of brake systems can exhibit both positive and negative gradients with respect to sliding speed, depending on the pad. A negative friction gradient is not the cause of the NVH behavior currently associated with mode coupling phenomena. The friction rule used here (Figure 2) has been selected as a simple means for inducing vibrations in the contact, aiding in the current investigations of local synchronization states in the boundary layer.

$$\mu_p = \left| \frac{M}{\pi} \cdot \arctan\left(200 \cdot v_p\right) \cdot \left(\frac{1}{0.25 \cdot |v_p| + 1} + 1 \right) \right| \tag{4}$$

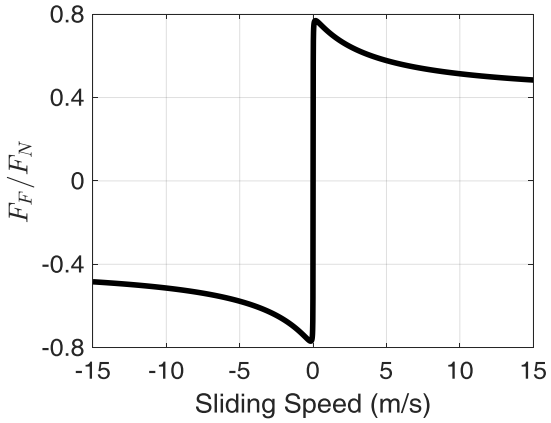

Fig. 2: Friction Rule Implemented at Patch-Disc Contacts (evaluated at $M = 0.8$)

This friction rule is designed such that the ratio F_F/F_N is differentiable at all sliding speeds, preventing numerical difficulties as the relative velocity passes zero, as implemented in Ostermeyer (2008). It is chosen in order to impose a friction curve that slowly decreases with increasing sliding speeds within the range of the average relative velocity between pad and disc for a given simulation. This condition is used for convenience, ensuring that the system is capable of exhibiting local stick-slip-like friction-induced vibrations of the contact plateaus. Thus the goal of characterizing synchronization states can be approached. This may ultimately be applied to various types of synchronized vibrations, regardless of the driving mechanism or friction assumptions.

For simplicity, Coulomb friction is implemented at points of contact between the disc and the brake pad *matrix material*, encompassing all parts of the pad's surface where patches are not present. For these pad-disc contacts, $\mu_{pad} = 0.3$ is implemented. For $M = 0.8$, the friction rule implemented for the patches asymptotically approaches $\mu_p = 0.4$ at its extrema, ensuring a nonzero difference between the friction coefficients of the pad-disc and patch-disc interfaces.

The global friction coefficient is computed as the ratio between the total sum of all local friction forces and the total sum of all local normal forces, as described in Ostermeyer and Merlis (2018). When there is no contact between the pad and disc, e.g. during pauses between brake applications, the convention $\mu = 0$ is established for the output data. In this work, the effective friction

radius is defined as the radial component of the centroid of the friction forces, and the friction torque is computed as the sum of all local friction moments about the disc's center.

2.1.3 The Multi-Timescale Problem

The time constants of the tribological processes simulated in the ACA span several orders of magnitude. To account for this, the ACA functionality is carried out on two distinct timescales. On the slower "low-frequency" (LF) timescale, processes such as patch dynamics, thermal effects, wear, and normal force distribution are computed with a time step $\Delta t = 0.01$ s. As high-frequency (HF) patch vibrations cannot be resolved on this timescale, they are computed on the HF timescale, with adaptive time steps on the order of $\Delta t \sim 10^{-9}$ s. During HF simulations, all LF processes are neglected and the associated simulation parameters are held constant. In *multi-timescale* simulations, the state of the ACA is saved at one or several instants during an LF simulation, and then processed on the HF timescale. Such simulations enable investigations e.g. into the effects of load history on friction-induced vibrations and synchronization. *Stand-alone* HF simulations can also be carried out, in which a pre-defined patch coverage state is assumed. This is useful for investigating specialized patch distribution cases.

The LF effects of patch dynamics on the global tribological behavior have often been discussed in the literature (e.g. Ostermeyer (2001)), and the corresponding interdependencies within the ACA are presented in Ostermeyer and Merlis (2018). The analogous HF interdependencies are summarized in Figure 3.

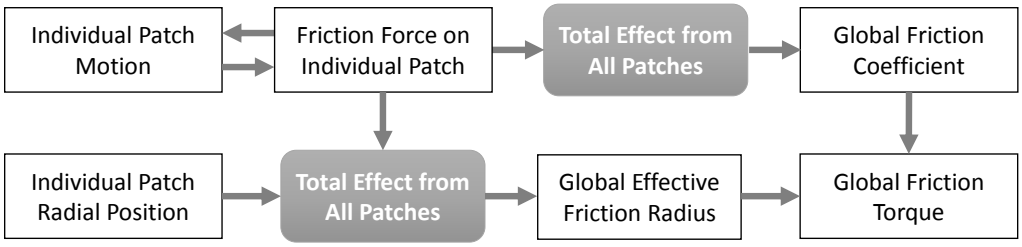

Fig. 3: General HF Interdependencies of Crucial Dynamics in the Tribological Boundary Layer

2.2 Quantifying the Synchronous Vibrations of Patches

In recent history, techniques for detecting and quantifying synchronized signals have been developed and widely employed in the fields of neuroscience. Tools such as phase-locking statistics Lachaux et al. (1999) and the phase-locking factor Sinkkonen et al. (1995); Palva et al. (2005); Slagter et al. (2009) primarily seek to determine the phase similarities of short, pulse-like oscillatory signals. By detecting the synchronicity of all signals relative to one another, these tools have provided the means for much progress in the associated fields.

The synchronization patterns of patches, however, are not necessarily uniform throughout the tribological interface. It is possible for multiple groups, or "islands," of patches to exhibit local synchronization behaviors. Depending on the sizes and distributions of these groups, relevant NVH events may still be excited by such synchronization states. This may be the case even if the synchronization islands have varying phase shifts and degrees of synchronicity in relation to one another. Some low-frequency global stick-slip behaviors may also be related to these HF synchronization islands. In order to adequately detect and quantify HF synchronization states of patches, an appropriate analysis tool is needed which is sensitive to such scenarios. Therefore, the aforementioned phase-locking techniques are not appropriate for the current work. While work has also been carried out towards analyzing nonuniform synchronization states, these are often developed for highly specified systems with a limited number of oscillators Stefański et al. (2007); Perlikowski et al. (2008).

The *Synchronization Index* $S(f)$ is introduced as a scalar value that seeks to quantify the synchronization state in the global contact area of an entire brake pad, encompassing many oscillating bodies. To this end, the motions of all patches are analyzed in the frequency domain via a Fourier analysis. The Synchronization Index for a given frequency is computed based an ABC Analysis Chu and Chu (1987); Partovi and Burton (1993) (also, Selective Inventory Control) of the phase angles of all patches vibrating at that frequency. It is developed based on the hypothesis that one or multiple highly prevalent phase angles can be indicative of synchronization. This is mathematically elucidated in the following description, in which a single arbitrary frequency is considered. In practice, the analysis is carried out over a wide band of discrete frequency bins.

The number of patches with an oscillation component at the given frequency are represented by Φ. The Synchronization Index is undefined for all frequencies at which fewer than two patches oscillate ($\Phi < 2$). A set of 180 evenly spaced phase bins are defined within the range $[-\pi, \pi)$. Each bin is assigned a value G equal to the number of patches whose phase shift is within the bin's range. A pseudo continuous consideration of similar phase shifts is achieved through applying a weighted moving average filter to the phase bins, using a Gaussian weighting function with a standard deviation of $2\pi/180$ rad and a window size of 3 bins. The processed bin data is then arranged in descending order, such that $G_1 \geq G_2 \geq G_3 \geq \cdots \geq G_{180}$.

The A group is separated from the B group at bin n_{AB}, defined as the minimum value satisfying

$$\sum_{i=1}^{n_{AB}} G_i \geq \tau_{AB} \cdot \Phi \,, \tag{5}$$

with the threshold value τ_{AB}. This is implemented with element precision rather than bin precision, i.e. n_{AB} is not necessarily integer value. The corresponding contribution S_{AB} to the Synchronization Index is computed as

$$S_{AB} = \frac{n_{AB,max} - n_{AB}}{n_{AB,max} - n_{AB,min}} \,. \tag{6}$$

Here, $n_{AB,max}$ is the theoretical maximum value of n_{AB} (worst case) for a given value of τ_{AB}, and $n_{AB,min}$ is the theoretical minimum value of n_{AB} (best case) for a given τ_{AB}, taking into account the effects of the weighted moving average filter.
An analogous computation is carried out for distinguishing the B and C groups:

$$\sum_{i=1}^{n_{BC}} G_i \geq \tau_{BC} \cdot \Phi \,, \tag{7}$$

$$S_{BC} = \frac{n_{BC,max} - n_{BC}}{n_{BC,max} - n_{BC,min}} \,. \tag{8}$$

The resulting Synchronization Index is computed as

$$S = S_{AB} \cdot w + S_{BC} \cdot (1 - w) \,, \tag{9}$$

with the weighting factor w. The result is a frequency dependent quantity which varies between 0 and 1, with lesser values resulting from more stochastic distributions of phase shifts, indicating poor synchronization, and greater values resulting from nearly identical phase shifts, indicating substantial synchronization. The functionality of the Synchronization Index is illustrated through theoretical minimal examples in the Appendix. For the preliminary analyses shown in this work, the parameter values $\tau_{AB} = 0.5$, $\tau_{BC} = 0.55$, and $w = 0.9$ are chosen.
The Synchronization Index is developed as a practical tool for the comparison of HF synchronization states. It is not intended to perfectly encapsulate all synchronization phenomena. It was designed to detect characteristic synchronization "islands" which often come about in relevant HF vibration scenarios. While there are certainly limit cases for which the Synchronization Index yields counterintuitive results (perhaps in the case of LF Schallamach waves), it is considered a useful tool to aid the interpretation of the results relevant to the current work.

3 Results

As described in Section 2.1.3, the ACA can be used to implement various types of studies towards analyzing friction-induced vibrations in tribological contacts. The results presented in this section are selected to exemplify various characteristic effects which are observable under particular simulation (or braking) conditions. These studies are aimed towards studying synchronized HF vibrations. Certain characteristic behaviors are investigated and identified towards inferring whether an NVH event may potentially be triggered, as discussed in Lee and Gesch (2009); Ostermeyer (2010). No statement is made towards the longevity of such behaviors based on these simulation results. To make such a claim would require HF simulations to be carried out over many simulation seconds, simultaneously accounting for all relevant LF phenomena. The results presented here emphasize the qualitative phenomena and dynamics rather than exact quantitative values.

3.1 Stand-Alone HF Simulations with Constant Parameters

First, stand-alone HF simulation results are presented in which predefined patch coverage states were implemented. The primary purpose of these initial studies is to demonstrate that established behaviors observed in scaled-down systems (as presented in Ostermeyer (2008, 2010)) can also be found in simulations of a full-scale brake pad. A parameter study was carried out over patch area and the friction model, as summarized in Table 1. In each study HF_{1-4}, 1758 patches were simulated in the contact

	$A_{p,mean} \approx 0.05$ mm^2	$A_{p,mean} \approx 1.25$ mm^2
$M = 0.8$	HF_1	HF_2
$M = 0.4$	HF_3	HF_4

Tab. 1: Stand-Alone HF Parameter Study Names

and the average sliding speed 10 m s^{-1} was implemented (corresponding to a vehicle speed of about 84 km h^{-1}). The patch areas were pseudorandomly selected from uniform distributions. For the simulations with smaller average patch sizes ($HF_{1,3}$), the areas were selected within $0.02 \leq A_p \leq 0.08$ mm^2. The simulations with larger patches ($HF_{2,4}$) employed areas based on $0.50 \leq A_p \leq 2.00$ mm^2. To heighten the effects of the patches' motion, the normal load was selected such that all patches were in contact with the disc, with the contact between the pad matrix and the disc minimized. This resulted in a surface pressure of about 44 kPa (brake line pressure about 1.32 bar, $F_N = 487.2$ N) for $HF_{1,3}$, and for $HF_{2,4}$ a surface pressure of about 1108 kPa (brake line pressure about 33.2 bar, $F_N = 12.37$ kN).
The time domain results from studies HF_1 and HF_2 are presented in Figures 4–5 and 6–7, respectively. In Figures 4 and 6 (top), the synchronization behavior of the patches is clearly observable. As the patches vibrate along the arc of the disc's rotation, the

instantaneous direction of the patches' motion is indicated through a color coding scheme. Red patches are moving with the local motion of the disc, and blue patches are moving opposite to the disc's motion.

It can be observed that macroscopic groups of patches move together in the same direction as their neighbors. These synchronized islands exhibit periodic behaviors that correspond well to the global friction dynamics. Figures 5 and 7 show how the friction coefficient's dynamics relate to further global system dynamics. The effect of patch vibrations on the global friction torque is expected to be more pronounced in the case of radially imbalanced synchronization patterns. Such cases should also be reflected through the effective friction radius. In these figures, an impression of the patches' motions is given through the sum of all patch velocities. Here, the total of all absolute velocities in reference to the stationary brake pad is used, not the total sliding speeds.

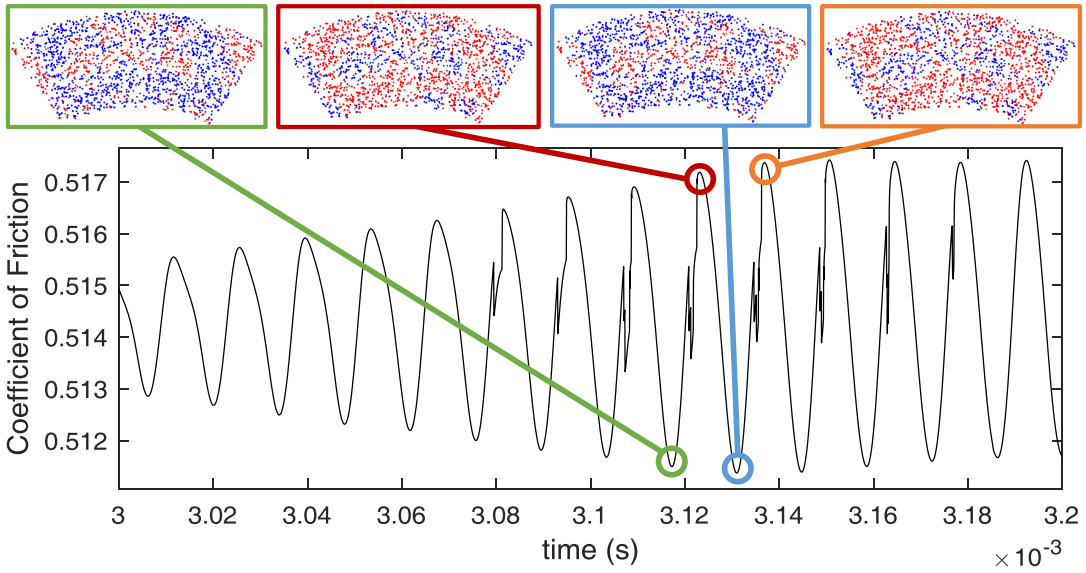

Fig. 4: HF_1: Influence of Patch Motion on Global Friction Behavior. (red) patches are moving with the local motion of the disc, (blue) patches are moving opposite **to** the disc's motion.

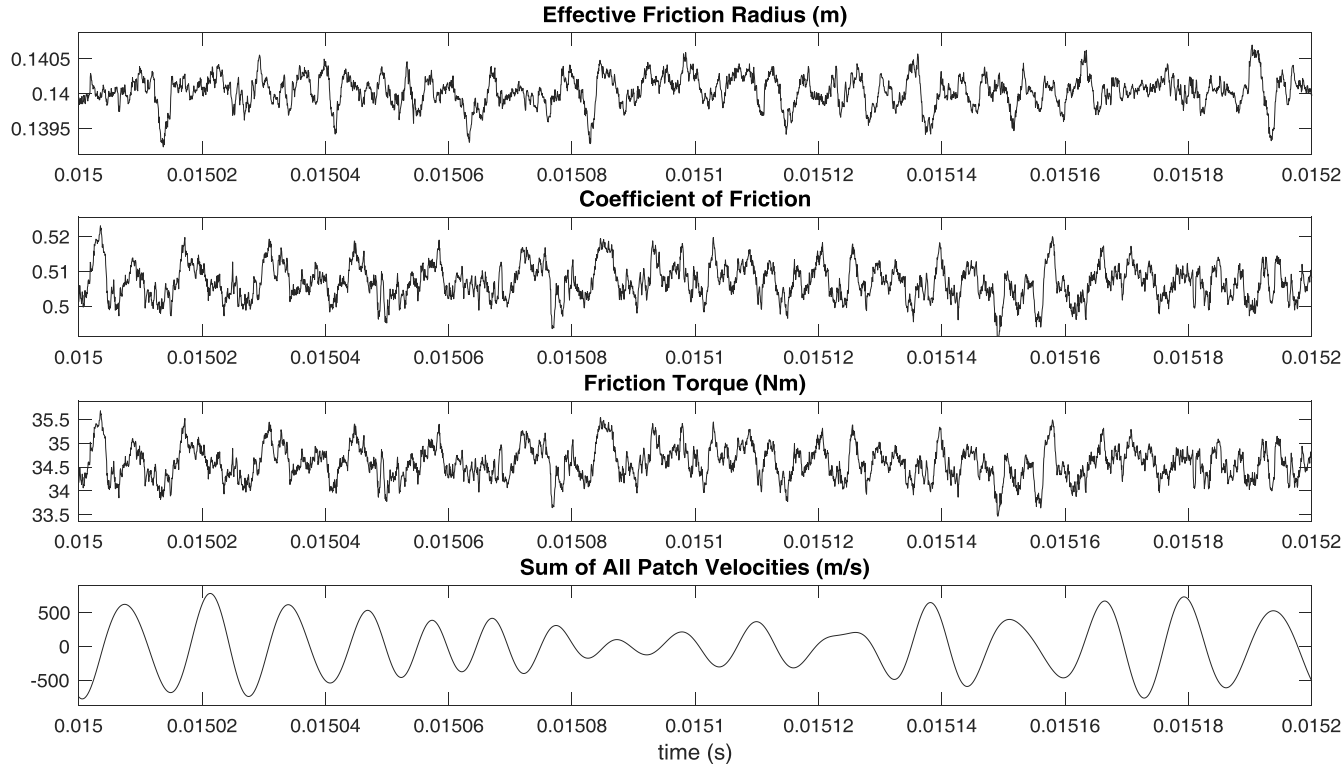

Fig. 5: HF_1: Global Tribological Data

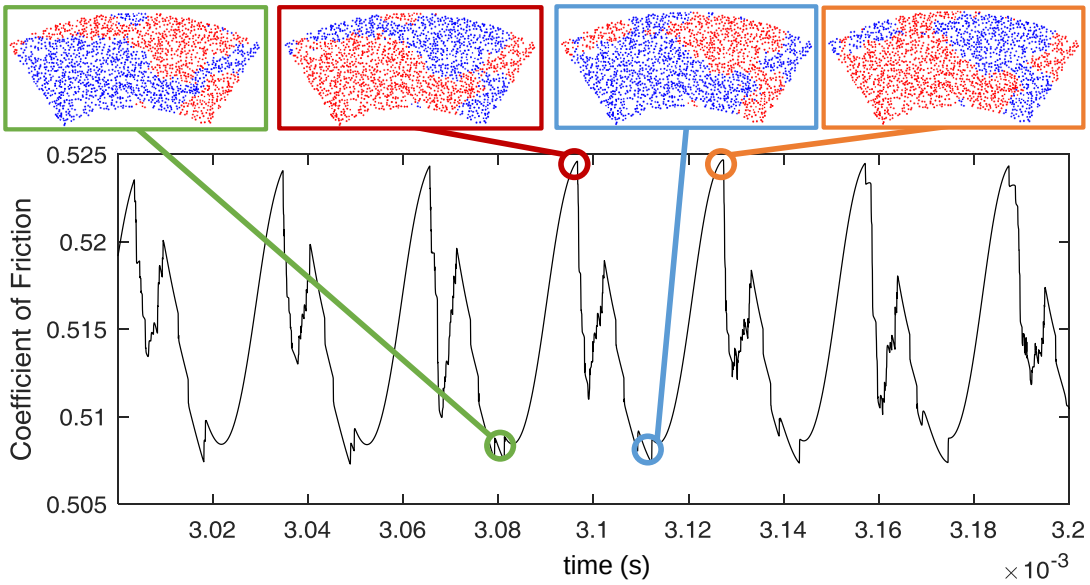

Fig. 6: HF_2: Influence of Patch Motion on Global Friction Behavior. (red) patches are moving with the local motion of the disc, (blue) patches are moving opposite to the disc's motion.

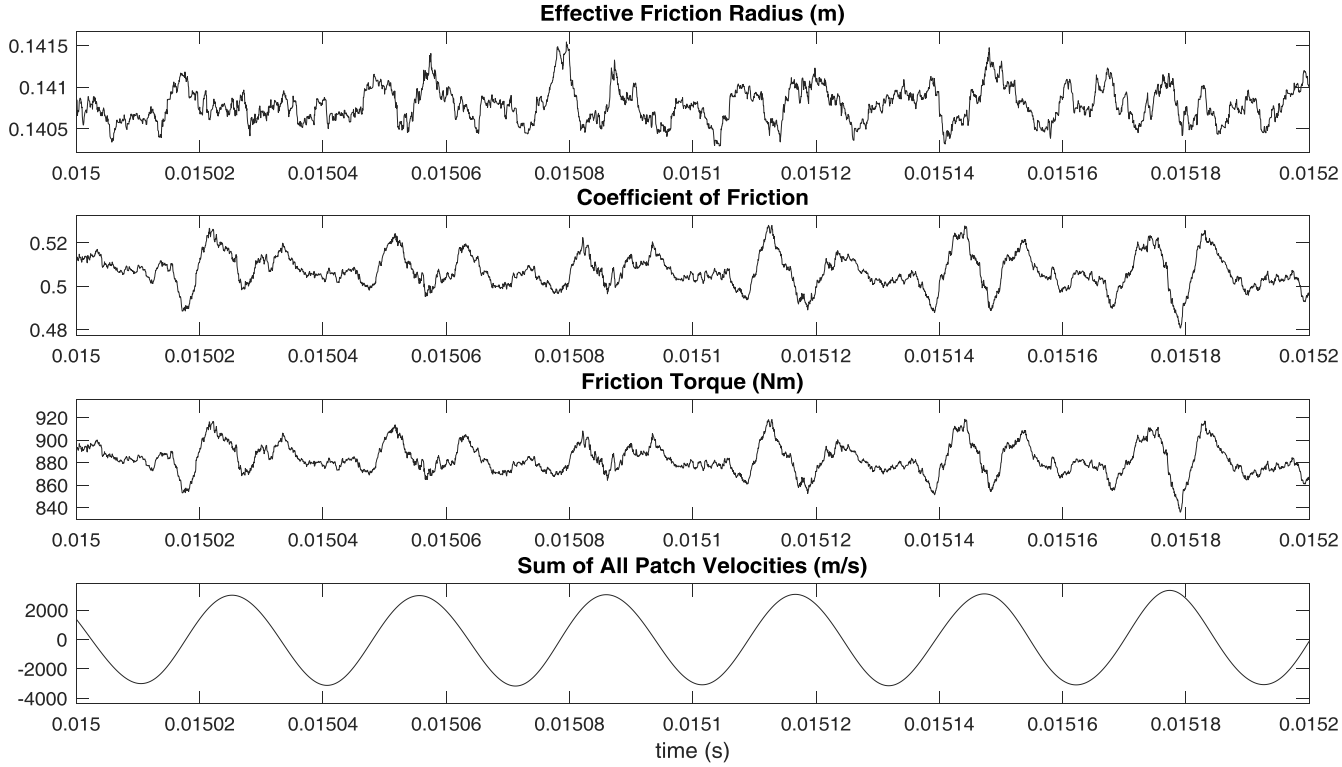

Fig. 7: HF_2: Global Tribological Data

As reflected in Eq. 3, the increase in patch area from HF_1 to HF_2 causes a stiffening of the coupling springs, yielding larger and better-defined synchronization patterns.

The frequency spectra of these global tribological results are shown in Figure 8 for all studies HF_{1-4}. Each amplitude spectrum is presented as a dimensionless quantity through normalization with respect to the time signal's DC offset. All Fourier analyses shown in this work were preprocessed with a Hann window. The corresponding Synchronization Index results are shown in Figure 9. At each relevant frequency bin, the *quality* of synchronization is represented through the Synchronization Index value, and the *prevalence* of the synchronization corresponds to the number of patches with substantial oscillation amplitudes (Φ from Section 2.2).

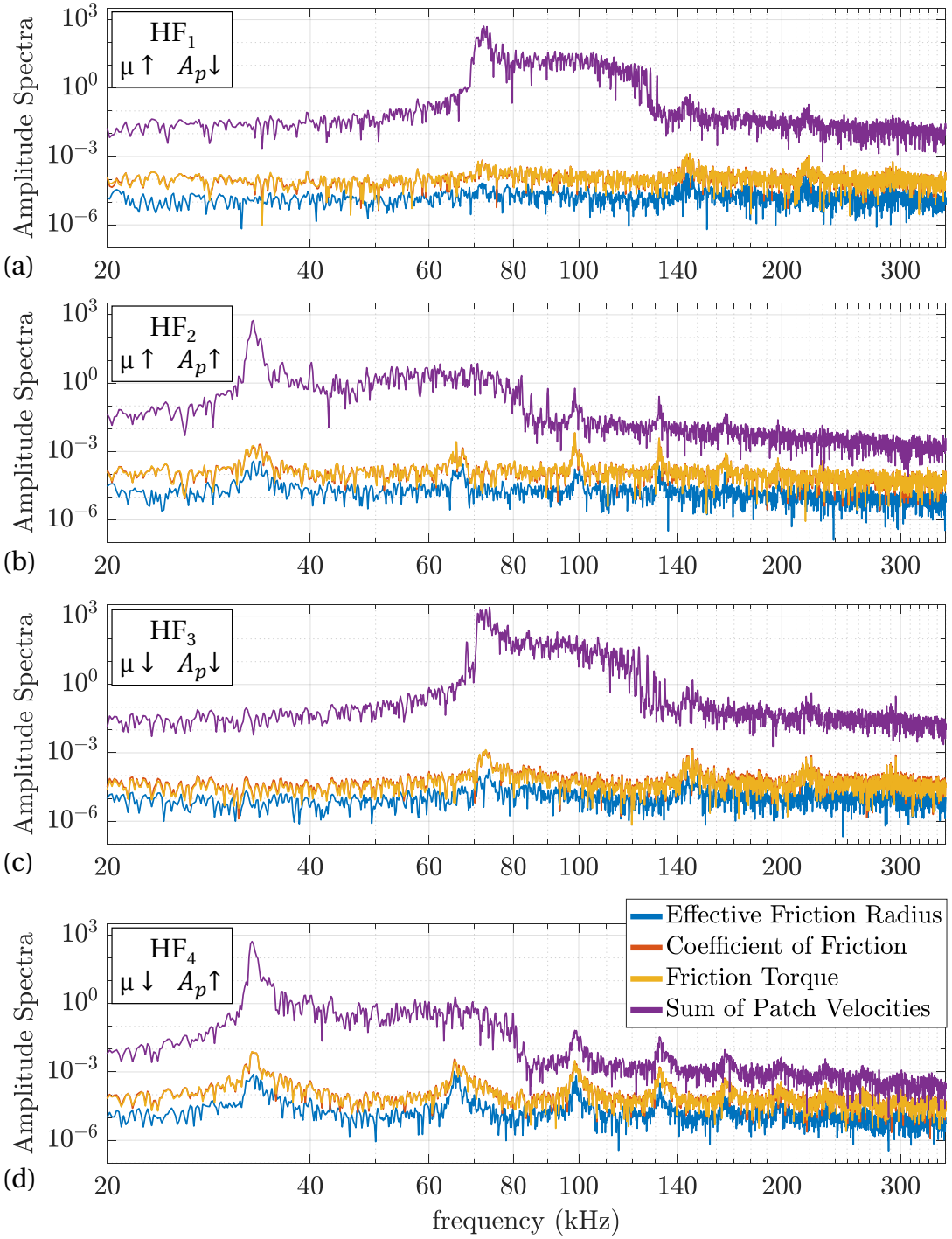

Fig. 8: Frequency Spectra of Stand-Alone Simulations. All results normalized to the mean value of the raw data. Note that the coefficient of friction and the friction torque exhibit very similar normalized behaviors; the corresponding curves are nearly completely overlapping.

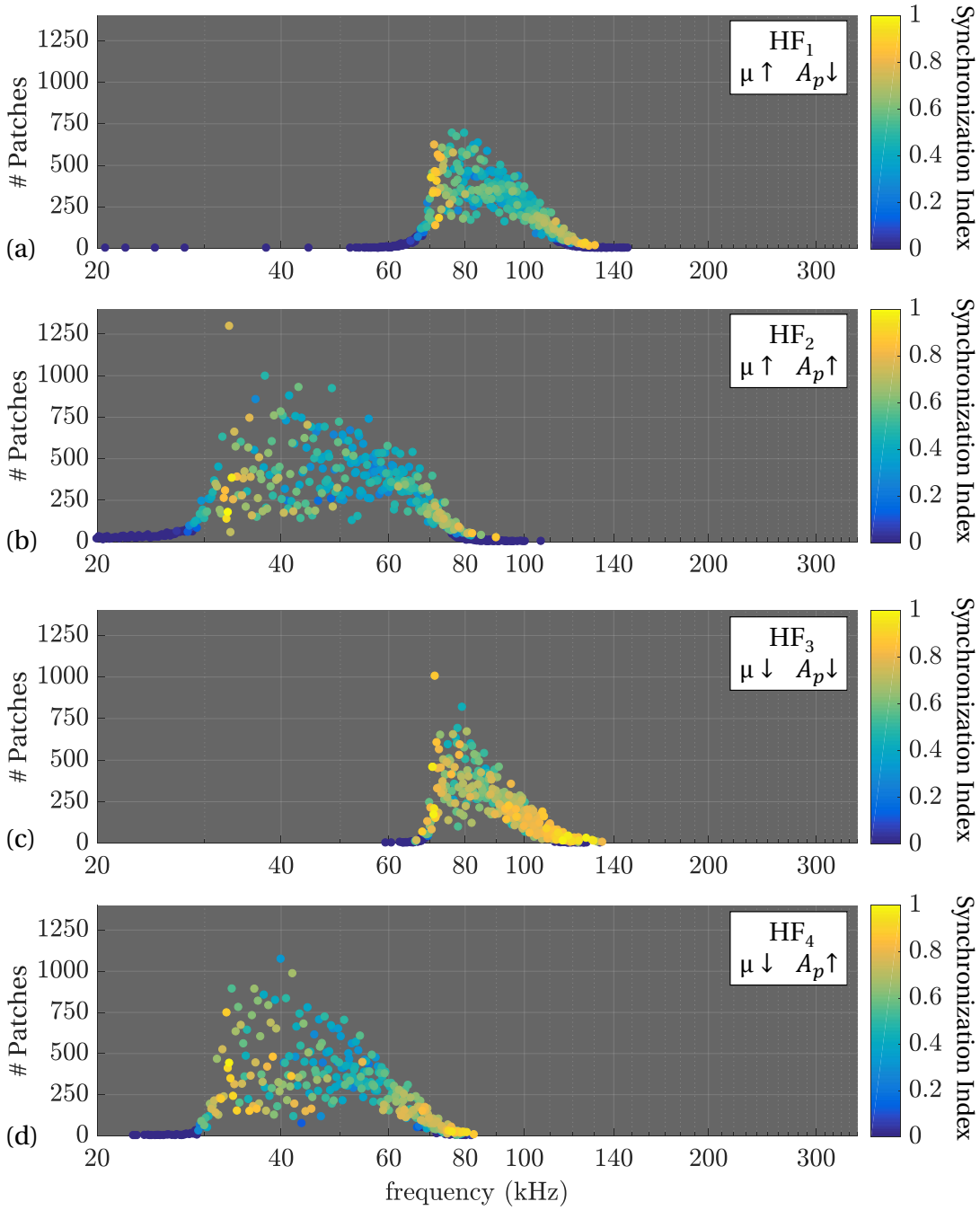

Fig. 9: Synchronization Index Results of Stand-Alone Simulations

In Figure 8, similar characteristic peaks of the global friction coefficient, friction torque, and effective friction radius are revealed, most of which are also present in the velocity spectra. The first peak of each velocity spectrum (around 73 kHz for HF_1 and HF_3, and around 32.8 kHz for HF_2 and HF_4) is significantly more pronounced than the other output quantities. In all four studies, these frequency peaks are followed by broad-band plateaus that are not observed in the other global outputs. These initial peaks and plateaus correspond well to the Synchronization Index results. It can be inferred that the corresponding friction peaks are caused by significant patch synchronization.

There are many peaks at higher frequencies in Figure 8 that do not correspond to any Synchronization Index results. These peaks are likely caused by the motions of individual, highly influential patches, and may partially be artifacts of the numerical Fourier transform.

Considering the effects of increased patch areas, the peaks of the HF_2 and HF_4 spectra have increased amplitudes, are narrower, and occur at lower frequencies than those from HF_1 and HF_3, respectively. Based on the implemented spring stiffness models, the approximate relationship between an isolated patch's natural frequency and its area $f_p \propto A_p^{-\frac{1}{4}}$ is expected. This is in good agreement with the frequency shifts observed in the spectral results and the Synchronization Indices.

The increase in patch area leads to more "spread out" Synchronization Index results, generally exhibiting increased prevalence values. Comparing HF_1 and HF_2, this size increase does not appear to significantly affect the synchronization quality. The synchronization quality increased significantly as a result of decreasing the friction coefficient for smaller patches. This effect is not as substantial, however, for the larger patches. It is a reasonable result that lower friction coefficients yield higher valued Synchronization Indices, as the friction forces are decreased relative to the forces of the coupling springs. As the patch areas

influence both the coupling forces and the normal forces, the effect of patch area on the patch synchronization is nontrivial and may be highly sensitive to certain relevant parameters.

Of these four studies, HF_4 exhibits the best agreement between the Synchronization Index results and the friction frequency spectrum. This may suggest an increased propensity for the triggering of an NVH event.

First interpretations of the combined effects of patch size and local friction values can also be made. Taking HF_1 as a reference, the HF_4 results can be interpreted as a combination of the changes observed in HF_2 and HF_3. For example, the Synchronization Index results of HF_4 are more spread out than HF_1 (influence of increased patch size), and are greater in value, especially at higher frequencies (influence of decreased friction coefficient).

3.2 Stand-Alone HF Simulation with Varying Patch Area

To gain further insights into the effects of patch area on the global friction response, a specialized study was carried out with nonconstant patch sizes. A patch coverage state comparable to that of HF_1 was generated at the start of the simulation. The patch areas were then gradually increased throughout the simulation once every 202 time steps, as indicated in Eq. 10

$$A_{p,t+\Delta t_{202}} = A_{p,t} + 10^{-6} \cdot \sqrt{A_{p,t}} \; . \tag{10}$$

This growth procedure was selected such that the final patch area distribution approximates that of HF_2 for a simulation about as long as HF_1. The simulation parameters were identical to HF_1, with the exception of normal pressure. The normal load from HF_2 was implemented to ensure that all patches maintain contact with the disc through the end of the simulation.

This is a theoretical investigation towards gaining preliminary insights into the system's transient response under varying conditions. It is not intended to reflect realistic patch growth rates.

Due to the chosen loading and patch area conditions, contacts between the pad matrix and the disc have a dominating influence on the global friction behavior at the start of this simulation. As the patches grow their effective spring stiffnesses increase, causing the patches to carry an increasing portion of the normal load. By the end of the simulation, the friction behavior is completely dominated by patch-disc contacts. This results in the development of the friction coefficient shown in Figures 10 and 11. The time domain global friction coefficient is shown alongside a corresponding short-time Fourier transform (STFT) in Figure 10. In Figure 11 a continuous wavelet transform (CWT) of the same signal is shown, offering a continuous impression of the development of the friction coefficient's frequency signature. Here, the decreasing frequencies of the characteristic peaks resulting from the increasing patch sizes are clearer to observe.

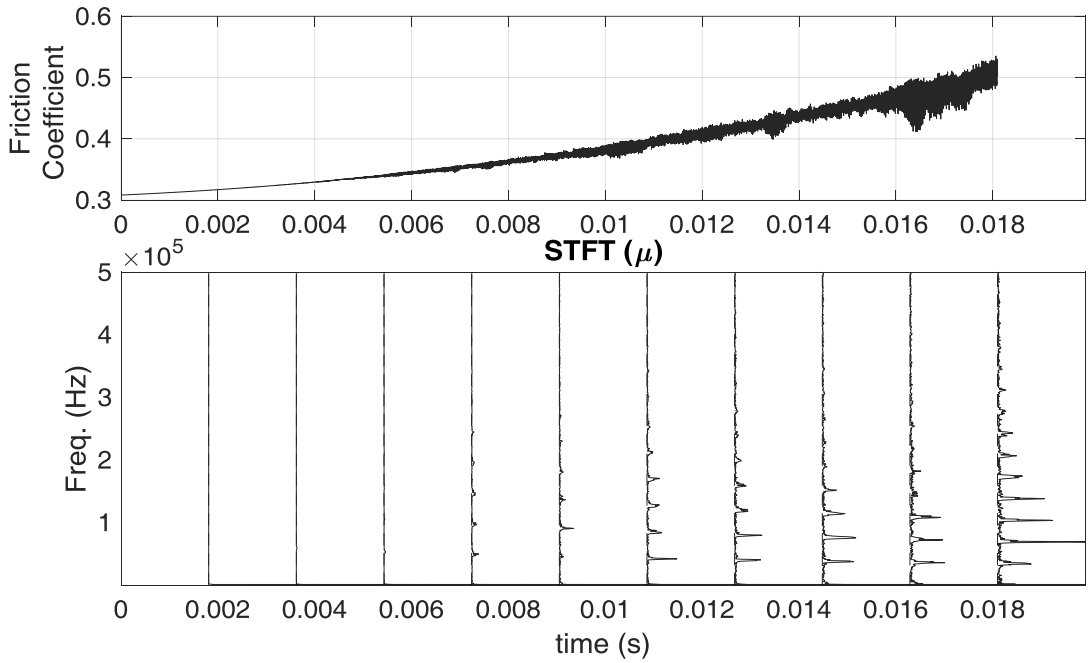

Fig. 10: (top) Time Domain Signal of the Global Friction Coefficient, (bottom) STFT Development of Dominant Peaks in the Frequency Signature of the Coefficient of Friction. STFT results are truncated below 10 Hz and then normalized to the maximum amplitde of about 0.004 (corresponding to the largest peak around 69.1 kHz)

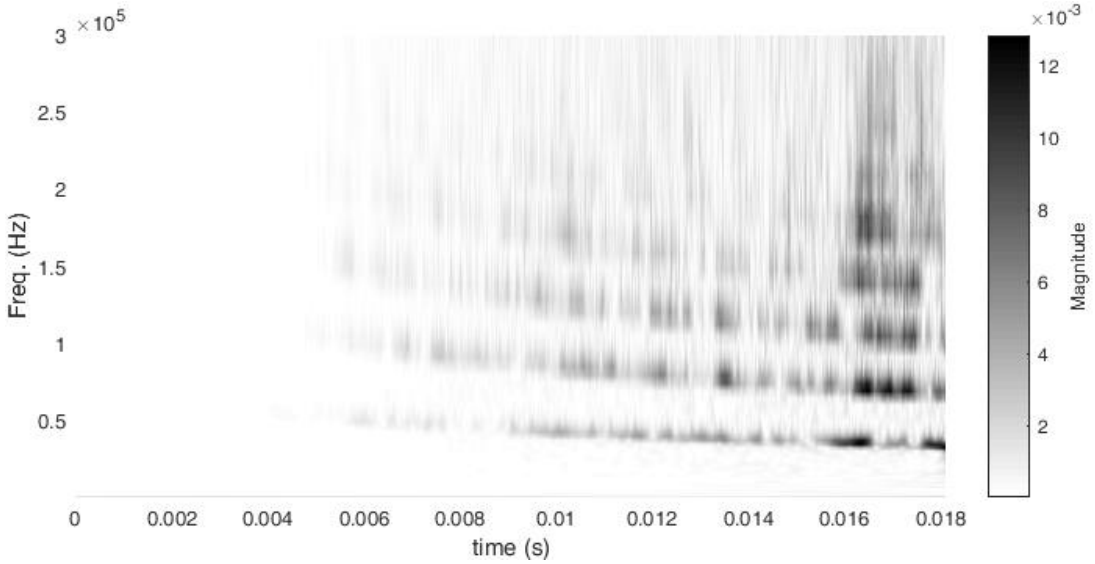

Fig. 11: CWT of the Global Friction Coefficient Resulting from Friction-Induced Vibrations and Patch Growth

As observed in the time domain results (Figure 10, top), the DC offset and the slow increase of the friction coefficient each have significantly greater magnitudes than the signal's HF oscillations. To aid in the interpretation of the HF results, the results at frequencies less than 10 Hz are omitted from all frequency domain output plots.
In both the STFT and CWT results, the emergence of individual dominant frequencies can be observed. The development of frequency signatures from stochastic (low-amplitude oscillations over a wide frequency range) to periodic (one or multiple dominant frequencies) is a documented triggering mechanism of NVH in brake systems Ostermeyer (2010). It is also relevant to note that friction peaks at a given frequency may also contribute to the onset of perceivable NVH events at differing frequencies Nishiwaki and Yamamoto (2018). It can be inferred that in physical brake systems, the transition from a pad-disc dominated state to a patch-disc dominated state could be related to the triggering of squeal. The development of synchronization states in this type of study will be investigated in a future publication.

3.3 Multi-Timescale Study

A multi-timescale study was carried out to investigate realistic braking scenarios that can potentially lead to relevant synchronized vibrations. The normal load variation shown in Figure 12 was implemented on the LF timescale. Each application had a duration of 10 seconds, separated by 5 second long pauses. The constant sliding speed $v = 10$ m s^{-1} and the friction model's multiplicative factor $M = 0.8$ were implemented throughout this study. HF analyses were carried out using the system states at the start and end of each application. During the HF simulations the patches' areas were held constant.

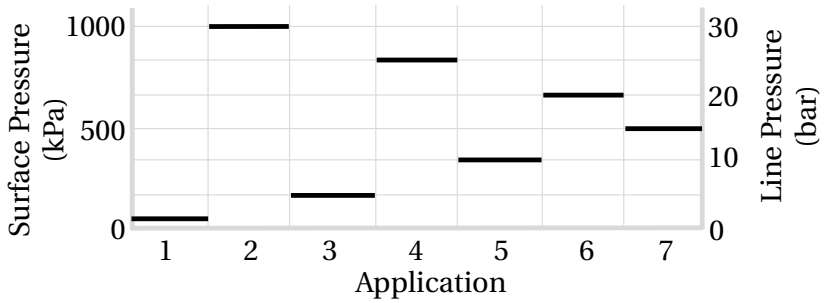

Fig. 12: Vibration Study Procedure, Based on the SAE 2521J Brake Squeal Module SAE International (2006)

The patch coverage states, global friction frequency spectra, and Synchronization Indices from a selection of the HF analysis results are presented in Figure 13.
Each point in the patch coverage state diagrams on left side of this figure represents a single patch. Based on a single simulation time step, the color coding of the instantaneous direction of motion of these patches offers a qualitative impression of the emergent synchronization patterns. While these patterns are not as clearly defined as those from the previous examples, a degree of local clustering can be observed. The results from the end of Application 3 (fourth row) indicate a correlation between this local clustering and the number of patches detected in the Synchronization Index analysis.
The friction coefficient oscillates with the greatest amplitudes during Application 3, in which a relatively low normal pressure was applied. The maximum amplitudes occurred at the beginning of this application, immediately following a high-load brake application. Here, the surface topography generated through Application 2 remains predominantly present, and is acted upon by the loading conditions of Application 3. Therefore, the friction-induced vibrations in the contact come about based on a patch coverage state similar to the one present at the end of Application 2, with excitation forces determined by the braking parameters

of Application 3. The increased oscillation amplitudes and individual high-valued Synchronization Index results (represented by yellow points) at the start of Application 3 may be of particular interest towards investigating brake squeal triggering mechanisms. At the end of Application 3, several medium to high valued Synchronization Index data points are present with increased prevalence (with regard to the number of associated patches). Some of these synchronization points are associated with amplitude peaks of the friction coefficient.

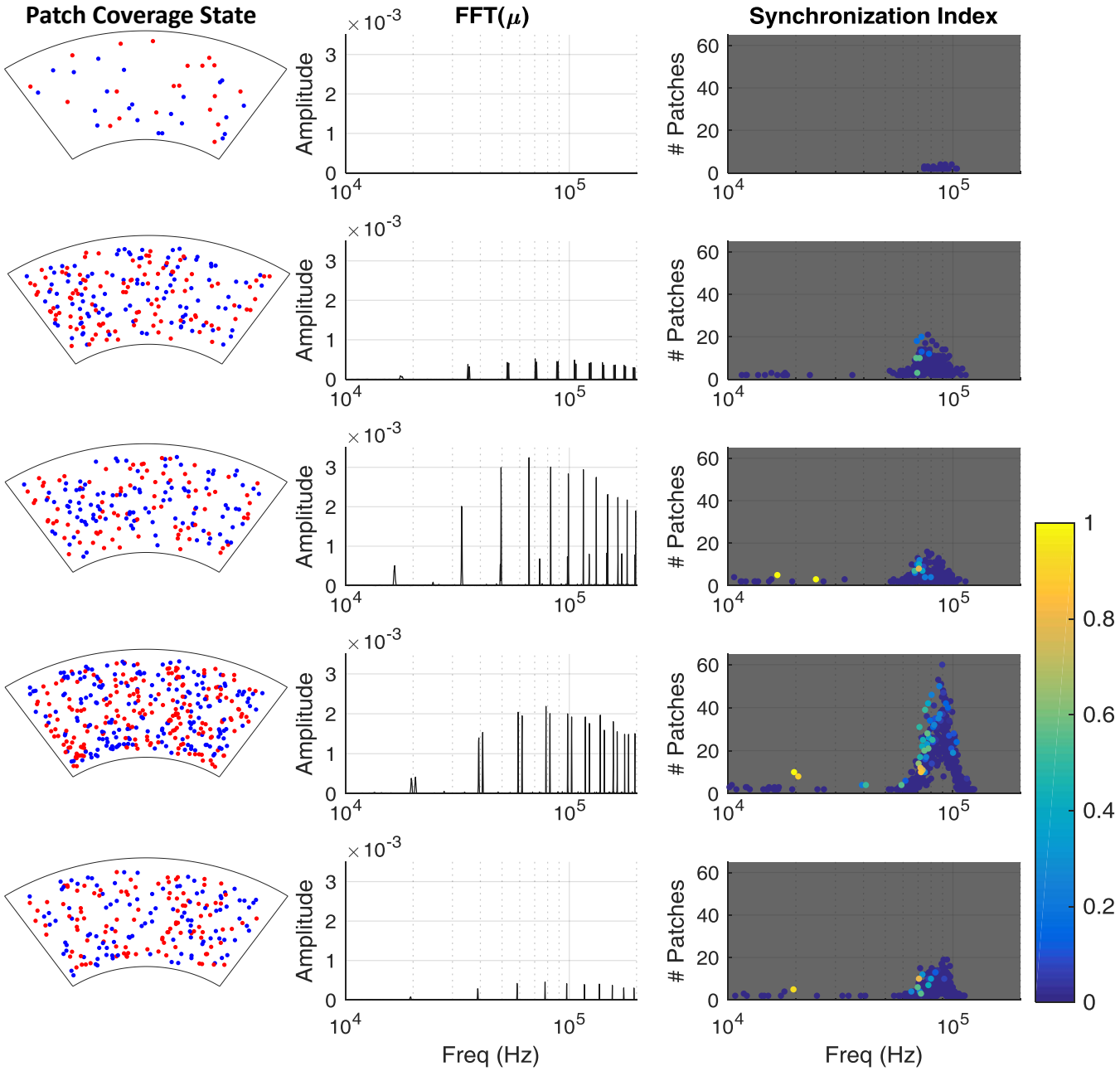

Fig. 13: Development of Multi-Timescale Results, **Top Row:** Beginning of Application 2, **Second Row:** End of Application 2, **Third Row:** Beginning of Application 3, **Fourth Row:** End of Application 3, **Bottom Row:** Beginning of Application 4. **Patch Coverage State:** (red) patches are moving with the local motion of the disc, (blue) patches are moving opposite **to** the disc's motion.

In general, significant interactions between the current braking parameters, load history, patch coverage state, synchronized vibrations, and global friction coefficient can be inferred. Distinct peaks in the friction coefficient's amplitude spectra occur at frequencies corresponding to both high-valued and highly prevalent Synchronization Indices. The friction spectral peaks that do not correspond to the Synchronization Index results are likely caused by the motion of individual, highly influential patches or numerical artifacts of the Fourier transform.

4 Discussion

Significant friction oscillations associated with low normal pressures can be the result of patch-disc contacts dominating the interactions. This was evidenced by the stand-alone HF simulation with varying patch area, and supported by the multi-timescale study. This may have implications for the triggering of brake squeal with low normal loads, particularly when there are many

patches present in the contact. This can come about if the low-load application causes the generation of many patches, or if a low-load brake application immediately follows an application in which several patches were generated. This is one example of the complex interactions between braking history and current braking parameters.

In general, the HF behavior at the beginning of a brake application is heavily influenced by the patch coverage state generated in the previous application by the previous set of braking parameters. This patch state is then excited with a new set of braking parameters. This new set of parameters may lead to an entirely different type of patch coverage state. In such a case, a variety of potential HF vibrational behaviors may come about as the new set of braking parameters excites a continuously developing patch state.

The exact influence of the Synchronization Index value, prevalence, and friction oscillation amplitudes on the triggering of NVH are unclear, although it is suspected that all three of these have some effect. For improved understanding of these issues, the sizes and spatial distributions of synchronization groups should be examined in the frequency domain, and the associated results should be applied to FEM simulations of the bulk pad and disc components to determine the associated excited vibrational modes.

Verification measurements should also be carried out. The characteristic friction and synchronization behavior simulated within the range 20–80 kHz is in good agreement with the measurements presented in Otto and Ostermeyer (2018).

5 Conclusions

Synchronized high-frequency patch vibrations are assumed to trigger squealing in automotive braking systems. Towards an improved understanding of the influences on squealing, these synchronized vibrations have been investigated using the ACA with the complexity of an entire pad-disc contact. Through a simplified model, it has been demonstrated how the onset of such synchronized vibrations can plausibly come about as a result of the braking history and the current braking conditions. It was also shown that the transition from a friction state dominated by pad-disc contacts to one dominated by patch-disc contacts can cause spectral peaks of the friction coefficient, a known NVH triggering mechanism.

Various means of analyzing simulation results have been presented, including the Synchronization Index which quantifies the synchronization of multiple oscillating patches. First results suggest that both the value and prevalence of the Synchronization Index are related to peaks in the frequency spectrum of the global friction coefficient. The Synchronization Index is not sensitive, however, to the spatial distribution of these bodies. Future works will introduce a new tool towards imaging the vibrations of many bodies with a focus on emphasizing local synchronization groups. The Synchronization Index will be integrated into this visualization scheme for a more robust interpretation of synchronization states. In this work, a preliminary set of Synchronization Index analysis parameters was chosen. Future investigations should be carried out towards the optimization of these values.

The scope of the simulations shown in the present work was to establish that the ACA is capable of depicting high-frequency synchronized vibrations. The Synchronization Index was introduced as a tool towards evaluating the associated phenomena and testing hypotheses. As a first step, the potential of these tools was illustrated. In future investigations, the ACA and Synchronization Index results should be validated with measurements.

Many aspects of the link between NVH and the high-frequency vibrations shown here are still not understood, although measurements indicate a close connection. In this work, a tool has been developed that is intended to aid in the determination of these correlations. Future investigations will consider realistic, spatially-resolved normal stresses on the pad. Further mesoscopic time scales will be implemented, which can also describe the temporal stability of the synchronization states. The latter is certainly necessary for detecting the triggering of low-frequency NVH oscillations. Additionally, this tool will be used towards identifying macroscopically measurable dynamics of the coefficient of friction in connection with the “elementary” friction processes on the individual patches. Thus, the local friction curve can be any arbitrary function of the velocity, if the vibrations of the patches are generated via mode coupling effects.

Further works will focus on the implementation of the ACA towards studying the vibrational effects associated with start and stop braking events. There, the transition between static and kinetic friction will come into the focus on both global and local spatial scales.

Acknowledgement

This research did not receive any specific grant from funding agencies in the public, commercial, or not-for-profit sectors.

Appendix

The functionality of the Synchronization Index is illustrated here using minimal examples. Here, only one isolated frequency bin is considered. To aid the presentation of these examples, only 10 phase bins are used rather than the 180 which are implemented for the simulation results shown in this work. The effects of the weighted moving average filter are neglected here. The analysis parameters are selected as follows: $\Phi = 100$, $\tau_{AB} = 0.50$, $\tau_{BC} = 0.55$, $w = 0.9$.

The following four theoretical cases are presented:

1. *Complete synchronization*: All patches are perfectly synchronous with one another.
2. One highly synchronous group is present, comprised of 75 patches. The remaining 25 patches do not belong to this synchronization island.
3. Multiple (3) synchronization islands are present, containing a total of 75 patches. The remaining patches do not belong to any of these islands.

4. *Perfectly asynchronous*: The patches' vibrations yield a uniform distribution of phase shifts.

The phase angle distributions associated with these cases are presented in Table A.1 and Figure A.1.

Tab. A.1: Phase bin values for four theoretical synchronization scenarios. Bins are arranged in order of descending value.

Bin:	G_1	G_2	G_3	G_4	G_5	G_6	G_7	G_8	G_9	G_{10}
Case 1:	100	0	0	0	0	0	0	0	0	0
Case 2:	75	3	3	3	3	3	3	3	2	2
Case 3:	27	25	23	4	4	4	4	3	3	3
Case 4:	10	10	10	10	10	10	10	10	10	10

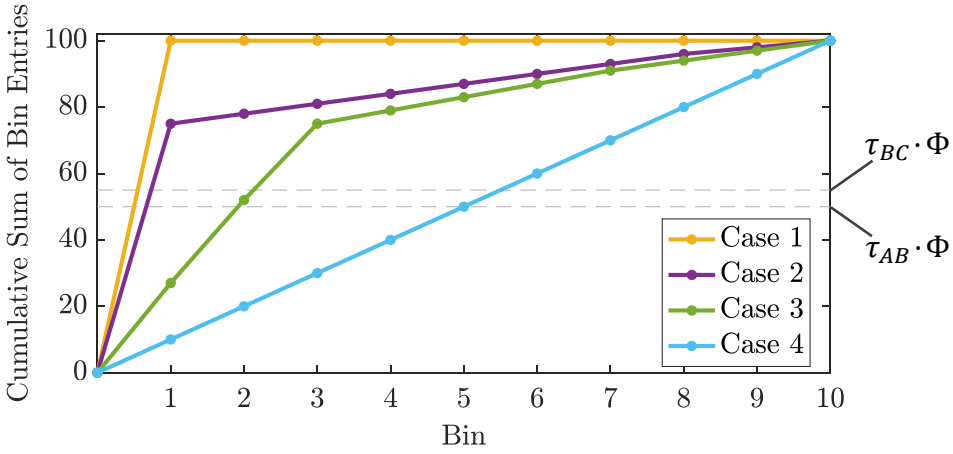

Fig. A.1: Phase bin values for four theoretical synchronization scenarios. The horizontal axis components of the intersection points between the cumulative sum curves and the dashed lines correspond to the respective values of n_{AB} and n_{BC}

Based on Eq. 5–Eq. 9, the corresponding Synchronization Analysis results are shown in Table A.2.

Tab. A.2: Synchronization Index results for the theoretical synchronization scenarios

Results:	n_{AB}	$n_{AB,max}$	$n_{AB,min}$	n_{BC}	$n_{BC,max}$	$n_{BC,min}$	S_{AB}	S_{BC}	S
Case 1:	0.500	5.000	0.500	0.550	5.500	0.550	1.000	1.000	1.000
Case 2:	0.667	5.000	0.500	0.733	5.500	0.550	0.963	0.963	0.963
Case 3:	1.920	5.000	0.500	2.130	5.500	0.550	0.684	0.681	0.684
Case 4:	5.000	5.000	0.500	5.500	5.500	0.550	0.000	0.000	0.00

These results illustrate the dependence of the Synchronization Index S on the synchronization state based on the associated phase angle distributions.

Nomenclature

Latin Symbols

A	Area (Surface, Contact, Cross Sectional)	(m^2)
c	Damping Coefficient	$(\mathrm{N\ s\ m}^{-1})$
D	Distance	(m)
f	Frequency	(Hz)
F	Force	(N)
G	Bin Value	(1)
k	Spring Stiffness	$(\mathrm{N\ m}^{-1})$
K	Constant Spring Stiffness Parameter	$(\mathrm{N\ m}^{-2})$
m	Mass	(kg)
M	Constant Factor of the Friction Model	(1)
n	Characteristic Result of ABC Analysis	(bins)
P	Patch	(1)
S	Synchronization Index	(1)
t	Time	(s)
v	Relative (Sliding) Velocity	$(\mathrm{m\ s}^{-1})$
w	Weighting Factor	(1)

Greek Symbols

Δt	Time Step	(s)
μ	Coefficient of Friction	(1)
Φ	Total Number of Patches	(Patches)
τ	Threshold Parameter	(1)

Symbols, Abbreviations, and Acronyms

$\propto$	Proportional to
$\sim$	On the order of
ACA	Abstract Cellular Automaton
CWT	Continuous Wavelet Transform
FEM	Finite Element Method
HF	High-Frequency
LF	Low-Frequency
NVH	Noise, Vibration, and Harshness
STFT	Short-Time Fourier Transform

Subscripts

AB	Distinguishing Group A from Group B
BC	Distinguishing Group B from Group C
C	Coupling
F	Friction
i, j	Arbitrary Index
max	Maximum Value
$mean$	Mean (Average) Value
min	Minimum Value
N	Normal
p	Patch
pad	Brake Pad Bulk Matrix Material
T	Tangential
0	Resting, Unloaded

Image Credits

Figure 1: Reprinted from Ostermeyer and Merlis (2018) (https://doi.org/10.3390/lubricants6020044) under the terms and conditions of the Creative Commons Attribution 4.0 International license (CC BY 4.0, http://creativecommons.org/licenses/by/4.0/)

References

Chao-Hsien Chu and Ying-Chan Chu. Computerized abc analysis: The basis for inventory management. *Computers & Industrial Engineering*, 13(1-4):66–70, 1987.

Tsutomu Hamabe, Ichiro Yamazaki, Kouji Yamada, Hiromichi Matsui, Shuuichi Nakagawa, and M Kawamura. Study of a method for reducing drum brake squeal. Technical report, SAE Technical Paper, 1999.

Norbert Hoffmann, Michael Fischer, Ralph Allgaier, and Lothar Gaul. A minimal model for studying properties of the mode-coupling type instability in friction induced oscillations. *Mechanics Research Communications*, 29(4):197–205, 2002.

Jean-Philippe Lachaux, Eugenio Rodriguez, Jacques Martinerie, and Francisco J Varela. Measuring phase synchrony in brain signals. *Human brain mapping*, 8(4):194–208, 1999.

Kwangjin Lee and JR Barber. An experimental investigation of frictionally-excited thermoelastic instability in automotive disk brakes under a drag brake application. *Journal of Tribology*, 116(3):409–414, 1994.

Li Lee and Earl Gesch. Discussions on squeal triggering mechanisms – a look beyond structural stability. In *SAE Technical Paper Series*. SAE International, 10 2009. doi: 10.4271/2009-01-3012. URL http://dx.doi.org/10.4271/2009-01-3012.

RI Leine, DH Van Campen, A De Kraker, and L Van Den Steen. Stick-slip vibrations induced by alternate friction models. *Nonlinear dynamics*, 16(1):41–54, 1998.

Augustus Edward Hough Love. *A Treatise on the Mathematical Theory of Elasticity*, volume 1. Cambridge University Press, 1892.

Masaaki Nishiwaki and Yukio Yamamoto. A study on trigger of small friction noise in disc brake squeal. Technical report, SAE Technical Paper, 2018.

G-P Ostermeyer. Friction and wear of brake systems. *Forschung im Ingenieurwesen*, 66:267–272, 2001.

G-P Ostermeyer. On tangential friction induced vibrations in brake systems. In *SAE International*, pages 101–111. 2008.

G-P Ostermeyer. Dynamic friction laws and their impact on friction induced vibrations. Technical report, SAE Technical Paper, 2010.

G-P Ostermeyer and Joshua Merlis. Effective simulation of the boundary layer of an entire brake pad. Number 2015-01-2664 in SAE Technical Paper, 2015. doi: 10.4271/2015-01-2664.

G-P Ostermeyer and M. Müller. New insights into the tribology of brake systems. *Proceedings of the Institution of Mechanical Engineers, Part D: Journal of Automobile Engineering*, 222(7):1167–1200, 2008. ISSN 0954-4070. doi: 10.1243/09544070JAUTO595.

Georg-Peter Ostermeyer and Joshua H. Merlis. Modeling the friction boundary layer of an entire brake pad with an abstract cellular automaton. *Lubricants*, 6(2), 2018. ISSN 2075-4442. doi: 10.3390/lubricants6020044. URL http://www.mdpi.com/2075-4442/6/2/44.

Johannes Otto and G-P Ostermeyer. Hochfrequente schwingungen in der reibgrenzschicht von bremssystemen. 15. Vibrometer Anwenderkonferenz. Polytec GmbH, 2018. (Publication Pending).

Satu Palva, Klaus Linkenkaer-Hansen, Risto Näätänen, and J Matias Palva. Early neural correlates of conscious somatosensory perception. *Journal of Neuroscience*, 25(21):5248–5258, 2005.

Fariborz Y Partovi and Jonathan Burton. Using the analytic hierarchy process for abc analysis. *International Journal of Operations & Production Management*, 13(9):29–44, 1993.

Yun Peng and Debao Zhou. Stress distributions due to a concentrated force on viscoelastic half-space. *Journal of Computations & Modelling*, 2(4):51–74, 2012.

Przemysław Perlikowski, Andrzej Stefański, and Tomasz Kapitaniak. 1:1 mode locking and generalized synchronization in mechanical oscillators. *Journal of Sound and Vibration*, 318(1-2):329–340, 2008.

K. Popp. Modelling and control of friction-induced vibrations. *Mathematical and Computer Modelling of Dynamical Systems*, 11(3):345–369, 09 2005. doi: 10.1080/13873950500076131. URL http://dx.doi.org/10.1080/13873950500076131.

SAE International. *SAE J2521-2006: Disc and drum brake dynamometer squeal noise matrix.*, 2006.

D Severin and S Dörsch. Friction mechanism in industrial brakes. *Wear*, 249(9):771–779, 2001.

J Sinkkonen, H Tiitinen, and R Näätänen. Gabor filters: an informative way for analysing event-related brain activity. *Journal of neuroscience methods*, 56(1):99–104, 1995.

Heleen A Slagter, Antoine Lutz, Lawrence L Greischar, Sander Nieuwenhuis, and Richard J Davidson. Theta phase synchrony and conscious target perception: impact of intensive mental training. *Journal of Cognitive Neuroscience*, 21(8):1536–1549, 2009.

Andrzej Stefański, Przemyslaw Perlikowski, and Tomasz Kapitaniak. Ragged synchronizability of coupled oscillators. *Physical Review E*, 75-1(016210):1–7, 2007.

B.L. Van de Vrande, D.H. Van Campen, and A. De Kraker. An approximate analysis of dry-friction-induced stick-slip vibrations by a smoothing procedure. *Nonlinear Dynamics*, 19(2):159–171, 1999.

Jens Wahlström. Towards a cellular automaton to simulate friction, wear, and particle emission of disc brakes. *Wear*, 313(1-2):75–82, 2014. ISSN 00431648. doi: 10.1016/j.wear.2014.02.014.

BA Wernitz and NP Hoffmann. Recurrence analysis and phase space reconstruction of irregular vibration in friction brakes: Signatures of chaos in steady sliding. *Journal of Sound and Vibration*, 331(16):3887–3896, 2012.